The Astrophysical Journal, 639:303–310, 2006 March 1

GRB 050117: SIMULTANEOUS GAMMA-RAY AND X-RAY OBSERVATIONS WITH THE *SWIFT* SATELLITE

Joanne E. Hill,[1,2] David C. Morris,[3] Takanori Sakamoto,[1] Goro Sato,[4] David N. Burrows,[3] Lorella Angelini,[1,5] Claudio Pagani,[3,6] Alberto Moretti,[6] Antony F. Abbey,[7] Scott Barthelmy,[1] Andrew P. Beardmore,[8] Vadim V. Biryukov,[9] Sergio Campana,[6] Milvia Capalbi,[10] Giancarlo Cusumano,[11] Paolo Giommi,[10] Mansur A. Ibrahimov,[12] Jamie Kennea,[3] Shiho Kobayashi,[3,13] Kunihito Ioka,[3,13] Craig Markwardt,[1] Peter Mészáros,[3] Paul T. O'Brien,[8] Julian P. Osborne,[8] Alexei S. Pozanenko,[14] Matteo Perri,[10] Vasilij V. Rumyantsev,[15] Patricia Schady,[16] Dmitri A. Sharapov,[12] Gianpiero Tagliaferri,[6] Bing Zhang,[17] Guido Chincarini,[6,18] Neil Gehrels,[1] Alan Wells,[3,7] and John A. Nousek[3]

Received 2005 July 13; accepted 2005 September 28

ABSTRACT

The *Swift Gamma-Ray Burst Explorer* performed its first autonomous, X-ray follow-up to a newly detected GRB on 2005 January 17, within 193 s of the burst trigger by the *Swift* Burst Alert Telescope. While the burst was still in progress, the X-Ray Telescope (XRT) obtained a position and an image for an uncataloged X-ray source simultaneously with the gamma-ray observation. The XRT observed flux during the prompt emission was 1.1×10^{-8} ergs cm^{-2} s^{-1} in the 0.5–10 keV energy band. The emission in the X-ray band decreased by 3 orders of magnitude within 700 s, following the prompt emission. This is found to be consistent with the gamma-ray decay when extrapolated into the XRT energy band. During the following 6.3 hr, the XRT observed the afterglow in an automated sequence for an additional 947 s, until the burst became fully obscured by the Earth limb. A faint, extremely slowly decaying afterglow, $\alpha = -0.21$, was detected. Finally, a break in the light curve occurred and the flux decayed with $\alpha < -1.2$. The X-ray position triggered many follow-up observations: no optical afterglow could be confirmed, although a candidate was identified 3″ from the XRT position.

Subject heading: gamma rays: bursts

1. INTRODUCTION

The *Swift Gamma-ray Burst Explorer* (Gehrels et al. 2004) was launched on 2004 November 20 to study gamma-ray bursts (GRBs) over a broad energy band covered by three instruments; a wide field of view gamma-ray burst alert telescope (BAT) and two narrow-field instruments (NFIs); an X-ray telescope (XRT), and a UV–optical telescope (UVOT). *Swift* slews rapidly to bursts detected by the BAT (Barthelmy et al. 2005), in order to point the XRT (Burrows et al. 2005) and UVOT (Roming et al. 2005) at the burst for rapid follow-up observations of the afterglow.

On 2005 January 17 at 12:52:36.037 UT, the *Swift* BAT triggered and located GRB 050117 (Sakamoto et al. 2005). For the first time, *Swift* responded autonomously to the BAT-triggered burst, pointing the XRT at the GRB while the burst was still in progress and allowing simultaneous gamma-ray and X-ray flux measurements of the prompt emission and follow up observations of the afterglow. The BAT light curve of the burst, which lasted 220 s, is multipeaked (Fig. 1). The XRT was on target and obtained a refined position and an image within 193 s of the BAT detection. The XRT detected the GRB at the end of the burst onset, measuring a source position of R.A. $= 23^{\rm h}53^{\rm m}53\overset{\rm s}{.}0$, decl. $= +65^{\circ}56'19\overset{''}{.}8$ (J2000.0; Hill et al. 2005a) and an absorbed flux of 1.1×10^{-8} ergs cm^{-2} s^{-1} in the 0.5–10 keV band. A faint afterglow was detected by the XRT during the subsequent orbits. The UVOT activation was not complete at the time of these observations, and therefore it remained in a nonobserving state throughout. No radio or optical afterglow was detected by the ground-based follow-up observations.

We report on the first autonomous repointing of an X-ray telescope to a newly discovered GRB, and describe the transition from the prompt emission to the afterglow.

2. GAMMA-RAY OBSERVATIONS

Ground analysis of the BAT event-by-event data produces an image significance of 54.2 σ and a refined GRB position within

[1] NASA Goddard Space Flight Center, Greenbelt, MD 20771; jhill@milkyway.gsfc.nasa.gov.
[2] Universities Space Research Association, 10211 Wincopin Circle, Suite 500, Columbia, MD, 21044-3432.
[3] Department of Astronomy and Astrophysics, 525 Davey Laboratory, Pennsylvania State University, University Park, PA 16802.
[4] Institute of Space and Astronautical Science/Japan Aerospace Exploration Agency, Building A, Room 1453, 3-1-1 Yoshinodai, Sagamihara, Kanagawa 229-8510, Japan.
[5] Department of Physics and Astronomy, The Johns Hopkins University, 3400 North Charles Street, Baltimore, MD 21218.
[6] INAF–Osservatorio Astronomico di Brera, Via Bianchi 46, 23807 Merate, Italy.
[7] Space Research Centre, University of Leicester, Leicester LE1 7RH, UK.
[8] Department of Physics and Astronomy, University of Leicester, Leicester LE1 7RH, UK.
[9] Crimean Laboratory of Sternberg Astronomical Institute, Moscow University, Russia.
[10] ASI Science Data Center, via Galileo Galilei, 00044 Frascati, Italy.
[11] INAF–Istituto di Astrofisica Spaziale e Fisica Cosmica Sezione di Palermo, Via Ugo La Malfa 153, 90146 Palermo, Italy.
[12] Ulugh Beg Astronomical Institute, Tashkent 700052, Uzbekistan.
[13] Center for Gravitational Wave Physics, Pennsylvania State University, University Park, PA 16802.
[14] Space Research Institute, Moscow 117810, Russia.
[15] Crimean Astrophysical Observatory, Ukraine.
[16] Mullard Space Science Laboratory, Holmbury St. Mary, Dorking, Surrey RH5 6NT, UK.
[17] Department of Physics, University of Nevada, Box 454002, Las Vegas, NV 89154-4002.
[18] Università degli studi di Milano-Bicocca, Dipartimento di Fisica, Piazza delle Scienze 3, I-20126 Milan, Italy.

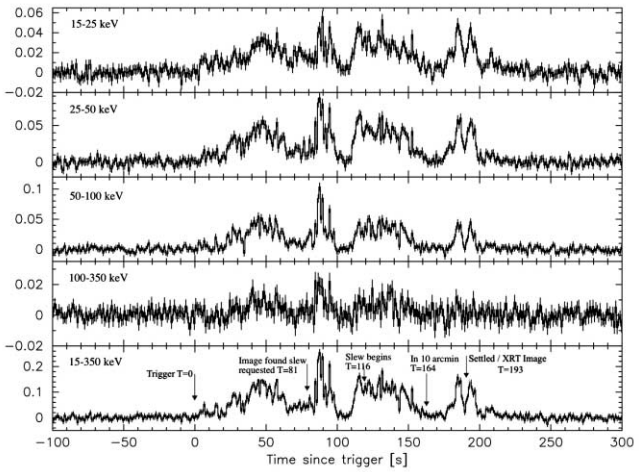

FIG. 1.—BAT energy-resolved light curve corrected to on-axis, in counts s^{-1} per fully illuminated detector.

10.″2 of the XRT position of R.A. = $23^h53^m53^s.1$, decl. = $+65°56'10''.3$, with an error circle radius of 45.″6 at 90% confidence level. Figure 2 shows the BAT error circle superimposed on the XRT image.

The burst prompt emission lasted 220 s, with T_{90} duration of 167.896 ± 0.004 s. This indicates that GRB 050117 is a relatively long burst when compared to the BATSE 4B revised catalog (Paciesas et al. 1999), where the logarithmic mean of the "long-burst" distribution ($T_{90} > 2$ s) is 27.2 ± 1.1 s, and only 46 out of the 1234 long bursts had T_{90} greater than 168 s. Instrument-to-instrument comparisons of burst durations may be susceptible to differences in detection thresholds (Kouveliotou et al. 1993), suggesting that the T_{50} duration may be more robust for this comparison. T_{50} for GRB 050117 was 84.796 ± 0.010 s, compared with the arithmetic mean T_{50} of the BATSE 4B revised distribution of 16.1 ± 1.7 s, indicating that GRB 050117 is in the upper 5% of the distribution.

The BAT background-subtracted light curve for the 15–350 keV energy band is shown in Figure 1 with annotations marking the

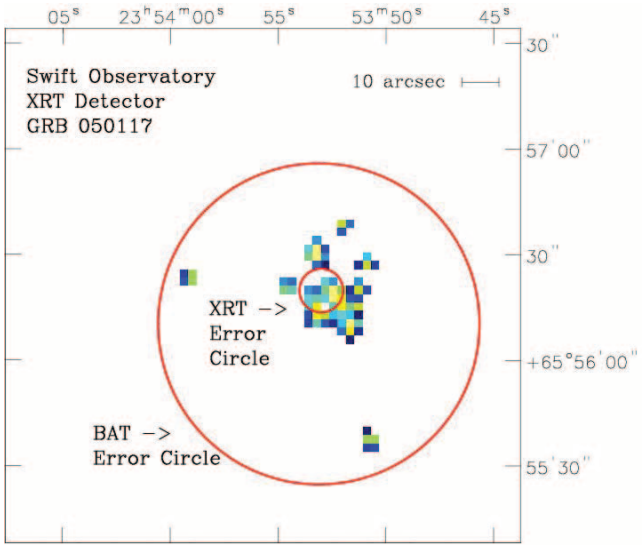

FIG. 2.—XRT Image of GRB 050117, showing the XRT 90% confidence error circle centered on the onboard position, corrected for a nonnominal spacecraft configuration, R.A = $23^h23^m53^s.0$, decl. = $+65°56'19''.8$, and BAT 90% confidence error circle from ground processing. The observed X-ray flux from this exposure is $(1.1 \pm 0.3) \times 10^{-8}$ ergs cm^{-2} s^{-1} in the 0.5–10 keV band.

TABLE 1
GRB 050117: ENERGY FLUENCE AND PEAK PHOTON FLUX MEASURED BY THE BAT

Energy Band (keV)	Energy Fluence[a,b] (ergs cm^{-2})	Peak Photon Flux[b,c] (photons cm^{-2} s^{-1})
15–25	$(1.17 \pm 0.04) \times 10^{-6}$	$(5.45 \pm 0.78) \times 10^{-1}$
25–50	$(2.40 \pm 0.05) \times 10^{-6}$	$(7.43 \pm 0.64) \times 10^{-1}$
50–100	$(3.44 \pm 0.08) \times 10^{-6}$	$(7.46 \pm 0.54) \times 10^{-1}$
100–150	$(2.33 \pm 0.10) \times 10^{-6}$	$(4.38 \pm 0.50) \times 10^{-1}$
Total	$(9.33 \pm 0.20) \times 10^{-6}$	(2.47 ± 0.17)

[a] Cutoff power-law model.
[b] 90% error.
[c] Simple power-law fit.

significant observatory events. Multiple peaks can be seen during the 220 s duration. The peak emission occurred 87.22 s after the trigger. By comparing the energy-resolved light curves (Fig. 1), it can be seen that the initial increase in count rate following the trigger occurred in the soft 15–25 keV band. Subsequently the burst became harder, with more than one-third of the total fluence in the 100–150 keV energy band. At the end of the gamma-ray phase, the emission appears to soften.

The BAT time-averaged spectra were fitted with two different models; a simple power-law model and a power-law continuum with an exponential cutoff (for the BAT energy band this is equivalent to the lower energy part of the Band function [Band et al. 1993]):

$$N_E(E) \propto E^{\gamma} \log [-E(2+\gamma)/E_{\rm peak}]$$

where $E_{\rm peak}$ represents the peak energy in the νF_ν spectrum and γ is the photon index. The fit was significantly improved using a cutoff power-law model, with an F-test probability of 3.5×10^{-6}. The time-averaged spectral fit over the 15–150 keV energy band gave a photon index of 1.1 ± 0.2 and an $E_{\rm peak}$ of 123^{+50}_{-22} keV with a $\chi^2 = 33.8$ for 56 degrees of freedom (yielding a null hypothesis probability of 0.992).

The burst total energy fluence was $(9.3 \pm 0.2) \times 10^{-6}$ ergs cm^{-2} in the 15–150 keV band in 220 s, with more than one-third of the fluence in the 100–150 keV band (see Table 1). The peak photon flux of 2.47 ± 0.17 photons cm^{-2} s^{-1} (integrated for 1 s from 15 to 150 keV using the best-fit model of a simple power law), occurred 87.22 s after the trigger.

Figure 3*a* shows the light curve obtained from the BAT in the 15–350 keV energy range. The light curve is divided into 17 time intervals encompassing each of the multiple peaks and troughs of the light curve. A spectrum was extracted for each time interval and fit with a simple power law corrected for the source angle and the respective BAT response. In the short time intervals, the statistics for the time-resolved analysis were not sufficient to warrant the use of a cutoff power-law model. The photon index from the simple power-law model spectral fit and the calculated flux for each of the time bins are shown in Figures 3*b* and 3*c*, respectively. Comparing the photon index with the flux, it can be seen that the spectrum is harder during the peaks of the burst than during the troughs, except for the final peak, where it is comparatively softer. The photon index from the power-law spectral fit is 1.8 ± 0.1 during the final peak, compared to ~1.2–1.4 during the previous peaks. It is during this final peak that the XRT data were obtained.

The BAT spectra below the break energy (15–100 keV) obtained at the time of the two simultaneous XRT measurements

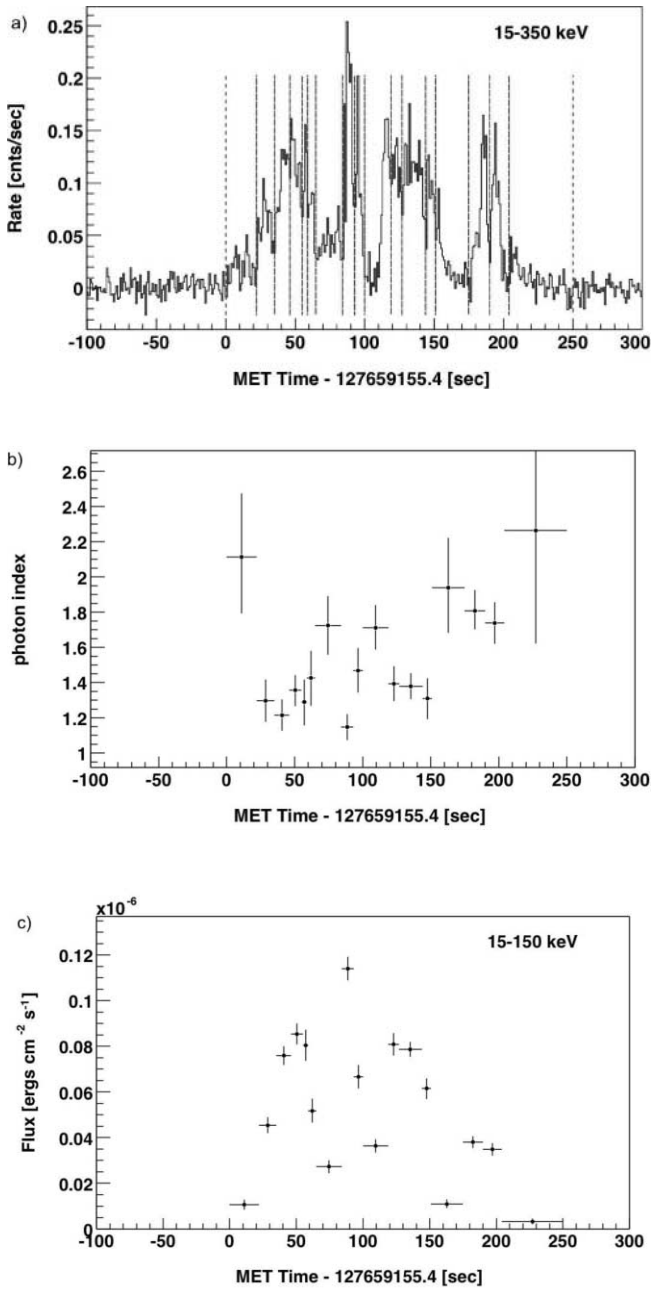

FIG. 3.—BAT time-resolved analysis, where MET 127659155.4 s is the trigger time. (*a*) Background-corrected light curve of GRB 050117, in counts s^{-1} per fully illuminated detector, corrected to on-axis. Dashed lines define the time bins for the analysis. (*b*) Photon index from a simple power-law fit from 15–150 keV, corresponding to time bins defined in (*a*). (*c*) Energy flux for 15–150 keV.

($\pm$0.5 s) were fit with a simple power law, yielding a photon index of 1.47 ± 0.14 and 1.49 ± 0.19 at the time of the image and photodiode mode data, respectively. According to the spectral fit and using the value of the Galactic $N_{\rm H} = 9 \times 10^{21}$ cm^{-2} (Dickey & Lockman 1990), the BAT flux was determined and extrapolated into the XRT 0.5–10 keV band; the results are shown in Figure 4. This process was repeated for each of the spectral fits for the 17 time bins shown in Figure 3; the flux for the 17 BAT time bins extrapolated into the 0.5–10 keV band are shown in Figure 5. The photon index obtained for the interval $t = 204$–250 s is not well constrained (Fig. 3*b*) and only produces an upper limit for the flux. For this reason, the photon index of 1.7 ± 0.1 obtained for the previous time interval ($t = 190$–204 s) was used to calculate the flux for $t = 204$–250 s and to calculate an upper limit for $t = 300$–913 s. Using the late time photon index of $2.3^{+0.9}_{-0.7}$ increases the flux and upper limit by a factor of 3.5.

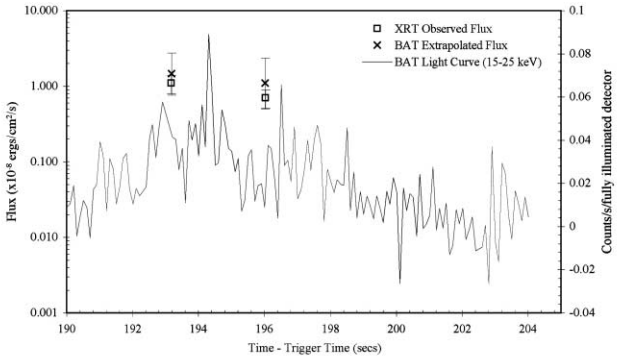

FIG. 4.—High-resolution plot of the simultaneous X-ray and gamma-ray observation of the prompt emission. The XRT observed flux from 0.5–10 keV, the BAT observed flux from 15–100 keV extrapolated into the XRT 0.5–10 keV band and the last peak of the BAT light curve in counts s^{-1} per fully illuminated detector. The BAT light curve is for the 15–25 keV energy band.

Analysis of the BAT data obtained after the end of the prompt emission ($t = 300$ s) through 913 s after the trigger, when the burst became constrained by the Earth for the NFIs, did not detect a source above a 3 σ detection level, corresponding to a flux upper limit of 8.5×10^{-10} ergs cm^{-2} s^{-1} between 15 and 150 keV for a spectrum corresponding to the previous time interval (photon index = 1.5).

3. X-RAY OBSERVATIONS

The XRT has several operating modes in order to maximize the science return according to the current observing sequence and the count rate from the burst. As soon as the observatory settles on a new burst the XRT acquires an image and, if the flux is greater than ~14 mcrab, determines the position of the burst. The position and a postage stamp image centered on the position

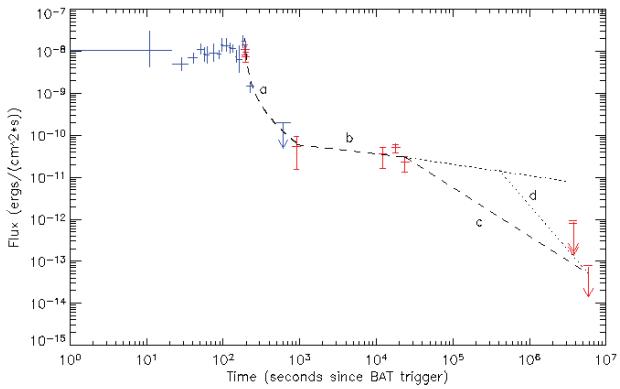

FIG. 5.—GRB 050117 light curve (absorbed fluxes). The BAT (*blue*) light curve using the spectral fits for each time bin and extrapolating the 15–100 keV flux into the 0.5–10 keV band (the flux and upper limit for the time intervals $t = 204$–250 s and $t = 300$–913 s were calculated using the photon index from $t = 190$–204 s) and the XRT (*red*) light curve (0.5–10 keV), showing the upper limits for the observations at more than 43 days after the burst. (*a*) A power-law fit assuming high-latitude emission from the internal shock, where $t_{\rm shock} = 187$ s and $\alpha < -1.2$. (*b*) A power-law fit to the afterglow decay with energy input from refreshed shocks assuming $t_0 =$ trigger time and $\alpha = -0.2 \pm 0.2$. (*c*) Continuation of the afterglow decay assuming a break in the light curve at $t = 6.6$ hr, $t_0 =$ trigger time, and $\alpha = -1.2$. (*d*) Extrapolation of $\alpha = -2$ from $t = 43$ days, showing the latest expected time of the break in the light curve at ~4.5 days ($t_0 =$ trigger time).

TABLE 2
A Summary of XRT Observations of GRB 050117

Orbit No. or Date[a]	Start Time (UT)	Stop Time (UT)	Live Time (s)	Time Since BAT Trigger (s)	XRT Mode
1[b]	12:55:49.24	12:55:49.34	0.1	193.2 s	Image
1[b]	12:55:52.42	12:55:52:53	0.109	196.0 s	PuPD
1[b]	13:07:36.2	13:07:47.4	11.2	900.2 s	LrPD/PuPD
3[b]	16:11:06.9	16:19:16.1	485	3.3 hr	LrPD/PuPD
4[b]	17:49:19.2	17:54:42.0	331	5.0 hr	LrPD/WT/PuPD
5[b]	19:27:53.7	19:29:28.5	119	6.6 hr	LrPD/WT
2005 Mar 2	00:12:43.8	05:27:45.3	7711	43.5 days	LrPD/PC
2005 Mar 26	13:15:38.8	05:35:57.8[c]	10 346	68.0 days	PC
2005 Mar 29	21:12:18.2	21:15:44.1	197	70.6 days	LrPD

[a] Source visibility during orbit 2 was entirely in the SAA and before SAA checking was disabled.
[b] 2005 January 17.
[c] 2005 March 28.

are telemetered through the Tracking and Data Relay Satellite System (TDRSS). In order to have sufficient full-scale response for very bright bursts, the energy per channel undersamples the spectrum in image mode, so that some spectral features are lost. The spectrum is expected to be piled-up, with more than one photon interacting in a pixel.

Following image mode the XRT switches into piled-up photodiode (PuPD) mode, which provides 0.14 ms timing resolution but no positional information and limited spectral information while the burst is bright. According to the source brightness, the XRT automatically switches between PuPD and the following modes; low-rate photodiode (LrPD) mode, where the flux is low enough to obtain spectral information and to update the on-board photodiode mode bias level; windowed-timing (WT) mode, providing lower timing resolution (1.8 ms) than the photodiode modes but acquiring a one-dimensional image and a high-resolution spectrum; and photon-counting (PC) mode, a more traditional mode of operation of an X-ray CCD camera. PC mode is only used when the source is extremely faint and provides limited timing resolution (2.51 s), a two-dimensional image, and high-resolution spectroscopy. Due to high background rates from the South Atlantic Anomaly (SAA) and the bright-Earth limb, the count rate evaluated by the XRT flight software was not sufficiently low to switch into PC mode during the initial observations. The XRT operating modes are described in detail in Hill et al. (2004, 2005), and a summary of the XRT observations of GRB 050117 is provided in Table 2.

GRB 050117 was within the NFI Earth constraint when it was first detected by the BAT. The observatory slewed when the burst became viewable by the NFIs 117 s later, arriving at the burst location 193 s after the trigger, by which time the observatory was in the SAA. The XRT obtained a 0.1 s image of the source immediately after *Swift* had settled on the burst and determined a position, which was within the BAT error circle. The observatory was still in its commissioning phase, and therefore the XRT onboard position was corrected on the ground for a nonnominal spacecraft configuration to give an updated position of R.A. = $23^{h}53^{m}53\overset{s}{.}0$, decl. = $+65^{\circ}56'19\overset{''}{.}8$ (J2000.0; Hill et al. 2005a). The estimated uncertainty in this position is $6\overset{''}{.}2$ (90% confidence).

Following the determination of the GRB position, XRT switched into PuPD mode at 12:55:51.409 and obtained high-resolution timing data for 109 ms before data collection was suspended by the onboard software to avoid flooding the telemetry with proton events from the SAA. There was a period of 2.752 s between the image mode data and the PuPD data when the instrument switched between modes and no data were obtained. The TDRSS postage stamp image, a thresholded, image and the PuPD mode data were obtained by XRT during the later portion of the gamma-ray phase of the burst (Fig. 1). The XRT onboard software determined that *Swift* had exited the SAA at 13:07:36.24, 900 s after the burst detection, and XRT obtained a further 11.15 s of PuPD mode data prior to the observatory slewing to a new source due to the approaching Earth constraint.

The location of GRB 050117 was very close to the *Swift* northern observing horizon and therefore was only visible outside of the Earth constraint for a very short period each orbit, the majority of which was while *Swift* was in the SAA. No data were telemetered during the second orbit for this reason. Before the third orbit, the XRT automated SAA checking was disabled to permit the XRT to collect data on the burst while in the SAA. By the sixth orbit, the orbital precession had placed the source continuously within the Earth constraint and no further observations were possible.

3.1. *Image Mode Analysis*

The burst was sufficiently bright at acquisition for the XRT to successfully obtain a refined position from a 0.1 s exposure image. The XRT image of the burst is shown in Figure 2.

The analysis described here refines the initial flux estimate (Hill et al. 2005a). A source spectrum cannot be extracted from the image, since more than 1 photon is expected to have interacted in a single pixel. A photoabsorbed power-law fit was obtained from the PuPD data immediately following the image, giving a photon index of 2.3 ± 0.5, assuming a Galactic absorbing column of 9×10^{21} cm^{-2} (Dickey & Lockman 1990) and $z = 0$ (the details of the spectral fitting are given in § 3.2). If one assumes the same source spectrum for the image mode data, a count rate can be inferred by dividing the total energy from the source in the image by the average energy of the assumed spectrum. Extracting the accumulated charge from the source in the $2'$ postage stamp image (defined as 3 σ above the background) and dividing by the average photon energy found from the model, a source count rate of 346 counts s^{-1} is determined. This count rate corresponds to an XRT observed flux of $(1.1 \pm 0.3) \times 10^{-8}$ ergs cm^{-2} s^{-1} (0.5–10 keV).

3.2. *Photodiode Mode Analysis*

The XRT photodiode mode data were complicated by two factors. First, the close proximity of the burst to the Earth limb resulted in an increased low-energy background in the data from the bright Earth. This was subtracted by postprocessing the data on the ground. The second complicating factor was the increase

TABLE 3

XRT Absorbed Flux Measurements (90% Confidence Intervals) of GRB 050117 in the 0.5–10 keV Band

Useful Exposure (s)	Start Time (since BAT trigger) (s)	Lower Limit (0.5–10 keV) (ergs cm^{-2} s^{-1})	XRT Flux (0.5–10 keV) (ergs cm^{-2} s^{-1})	Upper Limit (0.5–10 keV) (ergs cm^{-2} s^{-1})
0.100	193.2 s	0.8×10^{-8}	1.1×10^{-8}	1.4×10^{-8}
0.109	196.0 s	5.4×10^{-9}	7.3×10^{-9}	9.7×10^{-9}
11.1	900.2 s	1.5×10^{-11}	5.5×10^{-11}	9.5×10^{-11}
41.3	3 hr 18 minutes	1.6×10^{-11}	3.6×10^{-11}	5.1×10^{-11}
173.5	4 hr 57 minutes	3.8×10^{-11}	5.1×10^{-11}	6.1×10^{-11}
107.4	6 hr 35 minutes	1.3×10^{-11}	2.3×10^{-11}	3.1×10^{-11}
905.8	43.47 days	...	...	6.9×10^{-13}[a]
905.8	43.53 days	...	...	8.3×10^{-13}[a]
10 346	68.02 days	...	...	3.2×10^{-14}[a]
196.5	70.56 days	...	...	3.4×10^{-12}[a]

[a] No detection, 90% upper limit.

in background events due to passage through the SAA. A nickel line is observed in the spectrum, which is an instrumental effect created by interaction of protons in the SAA with the camera interior. The higher overall background level produced by the proton events during the SAA meant that the preliminary analysis of the timing and spectral data showed no evidence of emission due to GRB 050117. Analysis of XRT calibration data obtained in the SAA has shown that the overall background contribution to the spectrum during the SAA is proportional to the proton count rate measured as saturated pixels. This relationship was used to apply background correction to all the data sets on 2005 January 17, following the prompt image and PuPD data (the low number of proton events in the image and prompt PuPD data removed the need for such background corrections). Data were only included in the analysis if the number of saturated pixels (due to the SAA) contributed less than 1% of the total counts, yielding a total exposure of 333 s. The breakdown of the exposure analyzed for each orbit is shown in Table 3.

After correcting for the bright Earth and subtracting the background attributed to the SAA, the total number of counts with energy greater than 3 σ above the detector noise were calculated. The PuPD mode data had a sufficiently low count rate for one to assume that pile-up effects from the source are negligible and therefore it was possible to extract a count rate. The count rates obtained on 2005 January 17, where $t > 900$ s, were dominated by the calibration sources and the background contribution from other sources in the field was unknown. For these reasons, two short (approximately 4000 s) follow-up observations were performed by *Swift* 43 days after the burst. The first was with XRT in LrPD mode, to determine the counts attributable to the sky and instrument background, without contribution from the source. The second observation was in PC mode to provide two-dimensional imaging. Prompted by very late after-glow detections of other GRBs, an additional 20 ks observation was made of the GRB 050117 field, primarily in PC mode, 68 days after the burst. Four more short exposures were made in LrPD and PC mode, 71 days after the burst, when GRB 050117 was used as a "fill-in" target for the *Swift* observation schedule.

All data obtained in PC mode, between 2005 March 26 and March 28, were analyzed (>10 ks; grades 0–12). From the summed image, there was no detectable source above an upper limit of 3 σ above the background at the position of GRB 050117. The instrumental background is higher in LrPD mode than in PC mode, because the LrPD CCD readout scheme essentially integrates the entire field of view, including the calibration sources, into a single pixel. Based on the evidence that the source had faded below the detectable limit in PC mode, the short exposure LrPD mode data from 2005 March 29 were used to derive the expected background from the instrument and from the sky for earlier photodiode observations on 2005 January 17 and March 2.

For the follow-up observations, where there were a low number of source counts or no detectable source above 3 σ above the background, the expected background counts calculated from the final LrPD observation ($\sim$71 days after the burst) were used to derive 90% confidence intervals and upper limits on the source count rate in accordance with Kraft et al. (1991).

In order to compare the spectral distribution of the prompt X-ray emission with that from the BAT spectral fit, and to determine whether there was any obvious spectral evolution between the prompt and follow-up observations, a spectrum was extracted from the prompt PuPD mode data and a second spectrum was extracted from the data from each orbit following the prompt emission until 6.6 hr after the burst. Channels below 0.3 keV and above 10 keV were ignored and, in addition, channels containing lines from the calibration source and nickel K_α and K_β from proton interactions with the camera body were excluded from the analysis. A photoabsorbed power-law model ($z = 0$) with an absorption column density fixed to the Galactic value of $N_{\rm H} = 9 \times 10^{21}$ cm^{-2} was fit to both data sets.

From the prompt PuPD spectra, a photon index of 2.3 ± 0.5 was determined from a total of 28 counts with a minimum of 9 counts bin^{-1}, compared to the BAT photon index of 1.5 ± 0.2. Assuming the same photoabsorbed power-law spectrum with a photon index of 2.3 and a column density of $N_{\rm H} = 9 \times 10^{21}$ cm^{-2}, we obtain an absorbed flux of $7.3^{+2.4}_{-1.9} \times 10^{-9}$ ergs cm^{-2} s^{-1} for the 0.5–10 keV energy band. The 109 ms of photodiode mode data appear to be a continuation of the prompt emission seen in the 0.1 second image-mode exposure, at a slightly lower flux. A comparison of the simultaneous BAT and XRT measurements are shown in Figure 4. The XRT flux measurements obtained in image mode and photodiode mode of $(1.1 \pm 0.3) \times 10^{-8}$ and $7.3^{+2.4}_{-1.9} \times 10^{-9}$ ergs cm^{-2} s^{-1}, respectively, are within 90% confidence of the simultaneous BAT measurements extrapolated into the XRT band, of $1.5^{+1.3}_{-0.7} \times 10^{-8}$ and $1.1^{+1.3}_{-0.6} \times 10^{-8}$ ergs cm^{-2} s^{-1}, respectively.

For the follow-up data ($t > 900$ s), due to the low statistics, the spectra were rebinned with a minimum of only 10 counts bin^{-1}. A photon index of 2.0 ± 1.1 was obtained for a photoabsorbed power-law model and a column density of $N_{\rm H} = 9 \times 10^{21}$ cm^{-2}. This spectral fit was used to derive the fluxes or upper limits for

all data sets where $t > 900$ s. The confidence intervals for the fluxes were derived from the confidence intervals for the count rate and do not take into account the uncertainty in the spectral fit.

Both the prompt and the follow-up spectral fits indicate a possible low-energy contribution, which is not accounted for by a photoabsorbed power law with an absorbing column of the Galactic value. In addition, although the prompt and the follow-up spectral fits are comparable, when the count-rate hardness ratio for the data at ~200 s is compared with the hardness ratio for the data obtained between 900 s and 6.6 hr, the early data appear to have a harder spectrum. This suggests a spectral evolution from the early data to the later data, but there are too few counts to quantify this; however, we note that this inference from the hardness ratios is inconsistent with the photon indices obtained from the spectral fits. The X-ray fluxes derived from the BAT and the XRT spectral models, for both the early and the follow-up spectra, are consistent at the 90% confidence level between 0.5 and 10 keV. For this reason, and because the following discussion is not heavily dependent on the spectral analysis, a more rigorous spectral analysis for data with low statistics was not performed. The absorbed fluxes obtained from the XRT spectral fits with $N_{\rm H}$ fixed to the Galactic value (Table 3) are shown with the BAT absorbed fluxes from each of the 17 time intervals extrapolated into the 0.5–10 keV band in Figure 5. A smooth transition from the early gamma-ray emission to the X-ray emission is exhibited. Accounting for the Galactic absorption column, the unabsorbed fluxes are a factor of 2 higher. After the initial detection during the gamma-ray phase of the burst, a faint, slowly decaying afterglow is detected.

On 2005 January 17, a total exposure time of less than 15 s was accumulated in WT mode during which, there was no detectable source above the very high background. It is not possible to correct the bright-Earth contribution in the WT data using the same technique as for LrPD mode, and therefore these data were not included in the analysis.

4. FOLLOW-UP OBSERVATIONS

Follow-up observations were made at optical and radio wavelengths several hours, and in some cases days, after the burst trigger. A summary of those observations and the corresponding upper limits taken from GCN Circulars is given in Table 4.

A follow-up observation on 2005 January 17 16:58 with the 1.5 m telescope at Maidanak Astronomical Observatory identified a source candidate within the XRT error circle at R.A. = $23^{\rm h}53^{\rm m}52\overset{\rm s}{.}6$, decl. = $+65^\circ56'19\overset{''}{.}7$ (Fig. 6). The estimated source brightness, based on a total exposure of 1860 s taken in two epochs between 15:49 and 17:22, is $R = 23.6 \pm 0.7$. Follow-up observations were made on 2005 April 6 with the Crimean Astrophysical Observatory 2.6 m telescope. No object was found down to a limiting magnitude of 23.4 (3 σ) at the position of the source candidate. Due to low signal-to-noise ratio in the January 17 observations and the absence of the underlying galaxy in the April 6 observations the candidate source cannot be confirmed as the GRB counterpart.

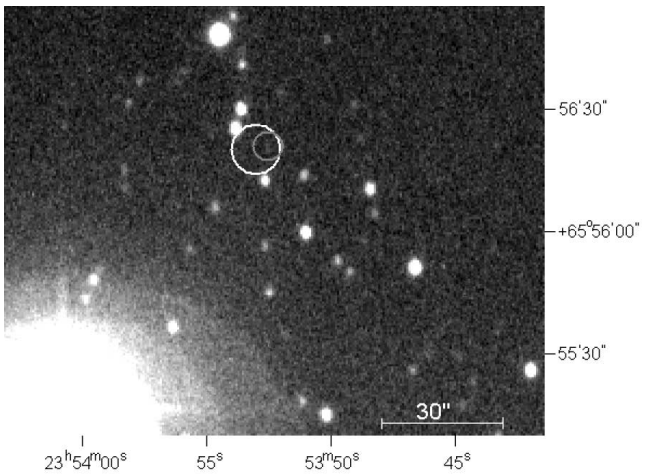

FIG. 6.—Image from the follow-up observation at the Mount Maidanak Astronomical Observatory in R band. The gray circle denotes the location of the possible source (limiting magnitude = 23.9 ± 1.3). The white circle is the XRT error circle.

The *Swift* UVOT was fully activated by the time of the late follow-up observations between 2005 March 26 13:15 and 2005 March 29 22:55. A total exposure of 15817 s was obtained with the V filter. From the co-added images, no source was detected in the XRT error circle down to a limiting magnitude of 21.38 (5 σ).

A lack of optical afterglow can be attributed to three reasons: the afterglow is intrinsically dark, there is dust extinction, or the burst has high redshift. Torii (2005) reported that the Galactic extinction is severe in the direction of the burst ($E_{B-V} = 1.7$ or $A_R = 4.6$) according to Schlegel et al. (1998), and therefore the lack of an optical counterpart is not surprising.

5. DISCUSSION AND CONCLUSIONS

The X-ray light curve is shown in Table 3 and Figure 5. The X-ray data indicate a decrease in flux of almost 3 orders of magnitude between the prompt emission at $t = 190$ s and the afterglow at $t = 900$ s. An initial steep decay of a similar magnitude over a comparable time period, as measured from the trigger time,

TABLE 4
GROUND-BASED FOLLOW-UP OBSERVATIONS OF GRB 050117

Telescope	Start Time (UT)	Filter	Duration	Upper Limit	References
14 ART (Osaka)	2005 Jan 17 14:05	I_c band	10×60 s	>17.5	Torii (2005)
MASTER Robotic Telescope (Moscow)	2005 Jan 17 14:58	Unfiltered	50×45 s	>19.0	Lipunov et al. (2005a, 2005b)
1.5 m (Maidanak)	2005 Jan 17 15:49	R band	1860 s	23.6 ± 0.7[a]	Karimov et al. (2005)
1.5 m (Granada)	2005 Jan 17 18:30	I band	6×300 s	>20.5	de Ugarte Postigo et al. (2005)
P200/WIRC Palomar Hale	2005 Jan 18 03:30	K_s band	32 minutes	>18	Fox et al. (2005), Berger et al. (2005)
VLA	2005 Jan 19 01:55	8.46 GHz	...	<130 μJy	Frail (2005)
	2005 Jan 24 03:21	8.46 GHz	...	<56 μJy	Soderberg & Frail (2005)
2.6 m, Crimean Astrophysical Observatory	2005 Apr 6 17:59	R band	3060 s	>23.4	

[a] Possible source identified.

has been observed in other *Swift* bursts; GRB 050319 (Cusumano et al. 2006), GRB 050126, and GRB 050219a (Tagliaferri et al. 2005), but in these cases the gamma-ray emission was over at the time of the X-ray observations. Similarly, the decay becomes significantly flatter over the following ~6 hr and then becomes steeper again sometime later in order to be undetected 43 days after the burst.

The XRT and extrapolated BAT fluxes obtained from the simultaneous XRT and BAT observations (Fig. 4) are within the 90% confidence limits. If we consider that the multiple peaks in the BAT light curve are attributed to internal shocks from the collision of the faster expanding shells with slower shells in front, then it is reasonable to assume that the X-ray flux at this time was also produced by an internal shock collision. The minimum expected emission following the peak from the internal shock is the high-latitude emission from the curvature effect (Kumar & Panaitescu 2000). The angular spreading timescale determines the decay timescale, and consequently the width of an internal shock peak, δt. Therefore, t_0 of the internal shock is, $t_{\rm shock} = t_{\rm peak} - \delta t = 195 - 8 = 187$ s. Due to the nondetection of gamma-ray flux between $t = 300$ and $t = 913$ s, we can assume that the X-ray flux after 900 s is dominated by the decaying afterglow and therefore we can use the XRT flux measurement at 900 s as an upper limit on the contribution from the decaying internal shock at this time. This provides a constraint on the temporal decay of the internal shock of $\alpha < -1.1$.

Following the end of the prompt emission, the light curve enters a shallower decay phase where, for the following 6.3 hr, there is very little decay in flux. The 90% confidence upper limit for the decay index is -0.5, but the best fit to the data is shallower than this: $\alpha = -0.21^{+0.28}_{-0.20}$. A second break in the power law is implied by the steep decay between the data points at 23 ks and the upper limit at 68 days. In order for the source to be undetected 68 days after the burst, the flux must decay with $\alpha < -1.2$ if the break occurred immediately after the last detection. If the break were later or the flux is significantly less than the upper limit, then the decay could be steeper.

A photoabsorbed power-law spectral fit to the prompt emission PuPD data ($t = 193$ s) using a Galactic $N_{\rm H}$ of 9×10^{21} cm^{-2} yielded a photon index of 2.3 ± 0.5. Fitting the same model to the summed LrPD and PuPD mode data from the afterglow ($t =$ 900 s–6.6 hr) yielded a photon index of 2.0 ± 1.1. For the X-ray data we assume a spectrum of the form $F(t, \nu) \propto (t - t_0)^{\alpha} \nu^{\beta}$ (Zhang & Mészáros 2004), where β is the spectral index and $\beta = 1 -$ photon index, yielding a spectral index of -1.3 ± 0.5 and -1.0 ± 1.1 for the prompt and follow-up observations, respectively.

The following sections discuss the possible theoretical interpretations of the observations.

5.1. *Early Emission* ($t < 1000$ s)

If the early emission is reviewed in the context of high-latitude emission from the internal shock then, taking the photon index of 2.3 ± 0.5 into consideration, where $\alpha = \beta - 2$ (Kumar & Panaitescu 2000), a decay of -3.3 ± 0.5 would be expected. This is within the constraints of the observation, where $\alpha < -1.1$.

The gamma-ray flux during the last internal shock (Fig. 3) decreases from $3.5^{+0.3}_{-0.3} \times 10^{-8}$ ergs cm^{-2} s^{-1} at 197 s to $3.3^{+1.4}_{-1.2} \times 10^{-9}$ ergs cm^{-2} s^{-1} at 227 s. Using $t_0 = t_{\rm shock} = 187$ s indicates a gamma-ray decay index of -1.7, or -2.1 taking the extremes of the 90% confidence limits. This is less steep than one would expect from high-latitude emission where, for a BAT photon index of 1.5 ± 0.2, $\alpha = \beta - 2 = -2.5$. To satisfy a decay of -2.5, t_0 would have to be further from the observed peak at 178 s. The observed flatter decay implies that there is an additional internal shock contribution of a lesser intensity. However, the decay is steep enough to be within the constraint determined in the X-ray regime. Due to the XRT and extrapolated BAT fluxes being of the same magnitude, one can assume that the X-ray flux during the prompt phase is dominated by the emission from the internal shock and any afterglow contribution, which one may expect at this time, cannot be detected. The expected afterglow decay may be in progress between the last internal shock and the flattening of the light curve at 900 s, but this cannot be concluded from these data.

Alternatively, if we fit a power law with $t_0 =$ trigger time to the two prompt measurements and the measurement at 900 s, we obtain a decay of $\alpha = -3.5^{+0.6}_{-0.8}$. Because there are no measurements between 190 and 900 s, this is an upper limit on the decay index and the decay could be steeper. If we consider that the early X-ray flux is from the afterglow, we see that the rapid decay is inconsistent with the spherical blast wave model, but the observed α/β relation may be consistent with the evolution of a jet (Sari et al. 1999). From the equations in Table 1 of Sari et al. (1999) if the X-ray frequency is below the cooling frequency ($\nu < \nu_c$), for a spectral index $\beta = -1.3$, we would expect a temporal index of $\alpha = 2\beta - 1 = -3.6$ indicating an electron energy distribution index of $p \sim 3.6$. The expected decay from the evolution of a jet is within 90% confidence limits of the observed decay, but the decay of the later emission ($t > 1000$ s) is much shallower than that which is expected after a jet break. If instead we assume $\nu > \nu_c$, we find the observed α is also inconsistent with an expected decay of -2.6.

5.2. *Late Emission* ($t > 1000$ s)

The shallow decay, $\alpha = -0.21^{+0.28}_{-0.20}$, may be explained by refreshed shocks, for which there are three possible mechanisms. The first is that the Lorentz factor has a power-law distribution, so that the slow shells pile up onto the decelerated blast wave to energize the shell (Rees & Mészáros 1998; Panaitescu et al. 1998; Sari & Mészáros 2000). Alternatively, the central engine may be continuously injecting energy with a (possibly) reduced rate (Zhang & Mészáros 2001). Finally, there may be collisions between the late injected shells and the decelerated fireball (Kumar & Piran 2000; Zhang & Mészáros 2002). In such a model one could expect undetected light-curve bumps if the Lorentz factor distribution or the outflow rate is very discontinuous.

This burst was long and multipeaked, and therefore if the later shells were slow moving with a modest Lorentz factor, energy would be injected into the afterglow as each shell collides into the external medium. This would cause rebrightening superimposed on the nominal afterglow decay and could explain the flatter than expected decay between 900 s and 6.6 hr. The light curve is not well sampled and so bumps, which may be expected from rebrightening, cannot be discerned from the light curve. The flattening of the light curve to a decay of -0.2 during this period and the observed α/β relation does not satisfy a simple synchrotron shock model outlined in Table 1 of Zhang & Mészáros (2004). The break in the light curve could be interpreted within the context of a simple afterglow model, satisfying the requirements of Table 1 of Sari et al. (1999), provided one can assume a small electron index of 1.3 if $\nu < \nu_c$ or 0.9 if $\nu > \nu_c$, and the large error on the spectral index is taken into account ($\beta = -1.0 \pm 1.0$). A mechanism for producing such flat electron indices has been discussed by Bykov & Mészáros (1996).

If the steepening is treated as the classical jet break due to the deceleration of the fireball, we can set limits on the width of the jet using the relation between jet break time and jet opening angle from Sari et al. (1999):

$$\theta_{\rm jet} = 10 \times \left[t_{\rm jet}({\rm hr})/6.2\right]^{3/8}.$$

If we assume that the earliest the jet break occurs is at the next to last 3 σ detection, 5 hr after the burst trigger, we calculate a jet angle of $\theta_{\rm jet} \sim 3^\circ$. Alternatively, we can assume that the jet break occurs between the last 3 σ detection at 6.6 hr and the upper limits at 43 days. If we assume a power-law decay index of -2 after the break (which is typical of postjet break decay indices) and extrapolate back from the upper limit at 43 days, we find that the break would have to occur at $t \sim 4.5$ days. This implies a jet opening angle of $\sim 10^\circ$. Jet angles of 3°–10° are consistent with typical GRB jet opening angles (Frail et al. 2001). We note, however, that the slope of the light curve between 900 s and 5 hr ($\alpha = -0.2$) is significantly flatter than that of the typical prejet break decay slope ($\alpha = -1$).

In the refreshed shock scenario, we assume that the afterglow due to ejected material colliding with the interstellar medium began at some early time while the prompt emission was still in progress for the observer. If the afterglow were sufficiently bright during the XRT observations at $t = 193$ s and $t = 196$ s, we would expect to see the afterglow emission superimposed on top of the internal shock emission, and thus a difference between the X-ray and extrapolated gamma-ray fluxes. We can estimate the expected flux contribution from the afterglow by assuming that the afterglow decays with a typical slope of $\alpha = -1$ prior to the onset of the refreshed shocks. If we project a power law with $\alpha = -1$ back from $t = 900$ s, we find that the expected contribution from the afterglow at $t = 196$ s is $\sim 3 \times 10^{-10}$ ergs cm^{-2} s^{-1}. This is an order of magnitude below the uncertainty in X-ray flux measurements at that time. Thus, any additional flux contribution from the afterglow in the XRT band pass at $t = 193$ s and $t = 196$ s is within the uncertainty of the flux measurement, and thus the presence of the afterglow at that time is not inconsistent with the data.

A steepening of the light curve is expected when all of the shocks have collided with the decelerating blast wave and the nominal decay is resumed. This is supported by the data where, in order for the afterglow to be undetected 68 days after the burst, the light curve must steepen to < -1.2 at some time after 6.6 hr.

5.3. *Summary*

The early X-ray light curve between $t = 193$ and $t = 900$ s is well explained by a simple internal shock mechanism, beginning at $t_0 = t_{\rm shock} = 187$ s after the burst trigger time and decaying with high-latitude emission, $\alpha < -1.2$. The afterglow due to the collision with the ambient medium may have started while the internal shock emission was still in progress, although the sample rate is too low to confirm this. The emission from the afterglow appears to be further enhanced by the additional input of energy from lagging shells of ejected material. The refreshed shock energy injection continues until at least 5 hr after the burst. Sometime between 5 hr and 4.5 days after the burst trigger, the refreshed shocks ceased and the light curve turned over to a steeper decay rate of $\alpha < -1.2$ corresponding to the expected afterglow decay; thus the burst was below the XRT detection threshold at $t = 68$ days.

To date, only 6% of the GRB observations by *Swift* have simultaneous gamma-ray and X-ray detections. The observations of GRB 050117 demonstrate the unique capability of *Swift* to observe both the burst and the afterglow in the X-ray regime.

This work is supported at Penn State by NASA contract NAS5-00136; at the University of Leicester by the Particle Physics and Astronomy Research Council on grant PPA/Z/S/2003/00507; and at OAB by funding from ASI on grant I/R/039/04. We gratefully acknowledge the contributions of dozens of members of the *Swift* team at PSU, University of Leicester, OAB, GSFC, ASDC, and our subcontractors, who helped make this Observatory possible and to the Flight Operations Team for their dedication and support.

REFERENCES

Band, D., et al. 1993, ApJ, 413, 281
Barthelmy, S., et al. 2005, Space Sci. Rev., 120, 143
Berger, E., et al. 2005, ApJ, 629, 328
Burrows, D. N., et al. 2005, Space Sci. Rev., 120, 165
Bykov, A. M., & Mészáros, P. 1996, ApJ, 461, L37
Cusumano, G. 2006, ApJ, 639, 316
de Ugarte Postigo, A., Sota, A., Jelnek, M., Gorosabel, J., Castro-Tirado, A. J., & Castro Cern, J. M. 2005, GCN Circ. 2957, http://gcn.gsfc.nasa.gov/gcn/gcn3/2957.gcn3
Dickey, J. M., & Lockman, F. J. 1990, ARA&A, 28, 215
Fox, D. B., Cenko, S. B., & Murphy, E. J. 2005, GCN Circ. 2960, http://gcn.gsfc.nasa.gov/gcn/gcn3/2960.gcn3
Frail, D. A. 2005, GCN Circ. 2963, http://gcn.gsfc.nasa.gov/gcn/gcn3/2963.gcn3
Frail, D. A., et al. 2001, ApJ, 562, L55
Gehrels, N., et al. 2004, ApJ, 611, 1005
Hill, J. E., et al. 2004, Proc. SPIE, 5165, 217
———. 2005b, Proc. SPIE, 5898, 313
Karimov, R., Ibrahimov, M., Kahharov, B., Asfandiyarov, I., Sharapov, D., Pozanenko, A., Rumyantsev, V., & Beskin, G. 2005, GCN Circ. 2958, http://gcn.gsfc.nasa.gov/gcn/gcn3/2958.gcn3
Kraft, R. P., Burrows, D. N., & Nousek, J. A. 1991, ApJ, 344, 355
Kouveliotou, C., Meegan, C. A., Fishman, G. J., Bhat, N. P., Briggs, M. S., Koshut, T. M., Paciesas, W. S., & Pendleton, G. N. 1993, ApJ, 413, L101
Kumar, P., & Panaitescu, A. 2000, ApJ, 541, L51
Kumar, P., & Piran, T. 2000 ApJ, 532, 286
Lipunov, V., et al. 2005a, GCN Circ. 2953, http://gcn.gsfc.nasa.gov/gcn/gcn3/2953.gcn3
———. 2005b, GCN Circ. 2954, http://gcn.gsfc.nasa.gov/gcn/gcn3/2954.gcn3
Paciesas, W. S., et al. 1999, ApJS, 122, 465
Panaitescu, A., Mészáros, P., & Rees, M. J. 1998, ApJ, 503, 314
Rees, M. J., & Mészáros, P. 1998, ApJ, 496, L1
Roming, P., et al. 2005, Space Sci. Rev., 120, 195
Sakamoto, T., et al. 2005, GCN Circ. 2952, http://gcn.gsfc.nasa.gov/gcn/gcn3/2952.gcn3
Sari, R., & Mészáros, P. 2000, ApJ, 535, L33
Sari, R., Piran, T., & Halpern, J. P. 1999, ApJ, 519, L17
Schlegel, D. J., Finkbeiner, D. P., & Davies, M. 1998, ApJ, 500, 525
Soderberg, A. M., & Frail, D. A., 2005, GCN Circ. 2980, http://gcn.gsfc.nasa.gov/gcn/gcn3/2980.gcn3
Tagliaferri, G., et al. 2005, Nature, 436, 985
Torii, K., 2005, GCN Circ. 2956, http://gcn.gsfc.nasa.gov/gcn/gcn3/2956.gcn3
Zhang, B., & Mészáros, P. 2001 ApJ, 552, L35
———. 2002 ApJ, 566, 712
———. 2004, Int. J. Mod. Phys. A, 19, 2385